International Journal of Multiphase Flow 36 (2010) 78–87

Contents lists available at ScienceDirect

International Journal of Multiphase Flow

journal homepage: www.elsevier.com/locate/ijmulflow

Blockage of constrictions by particles in fluid–solid transport

Jianjun Dai *, John R. Grace

Department of Chemical and Biological Engineering, University of British Columbia, 2360 East Mall, Vancouver, BC, Canada V6T 1Z3

ARTICLE INFO

Article history:
Received 22 February 2008
Received in revised form 10 April 2009
Accepted 7 August 2009
Available online 13 August 2009

Keywords:
Particulates
Hydraulic conveying
Constriction
Blockage
Particle feeding

ABSTRACT

Blockage is an important phenomenon in particulate flow. Work was undertaken to provide a better understanding of key hydrodynamic multiphase flow factors which cause, or contribute to, stalling and blockage in particulate feeding systems such as those used for feeding biomass into reactors. Rubber and plastic particles were hydraulically conveyed along a horizontal rectangular duct leading to constrictions of different geometries. Experimental results showed that large size, irregular shape, high volumetric concentrations of particles, small constriction dimensions and particle compressibility all increased the likelihood of blockage. Reynolds number also had a significant effect on particle behaviour and blockage propensity. The pressure drop needed to break a blockage is also considered, based on a simple horizontal packed bed model.

1. Introduction

When particles are conveyed by liquid and gases, for example in hydraulic or pneumatic feeding of reactors or conveyors, it is common for constrictions to be present to control, divert or split the flow. Serious problems can occur when the particles block the constrictions, leading to momentary or prolonged interception of feeding and conveying. These problems are especially critical and serious when conveying large and irregular particles, such as biomass particles which are of increasing interest in the development of new energy processes with reduced greenhouse gas emissions.

Experimental study and modeling of flow, both laminar and turbulent, in rectangular ducts of different aspect ratios have been widely conducted in past decades (e.g. Sparrow et al., 1967; Fleming and Sparrow, 1969; Beavers et al., 1970; Melling and Whitelaw, 1976; Gessner and Po, 1976; Kaushal and Tomita, 2003). A detailed literature review of flow regimes in rectangular channels with a narrow gap was given by Wilmarth and Ishii (1994). Experimental analysis of turbulent flow structure in a fully developed rib-roughened rectangular channel with PIV has been conducted by Islam et al. (2002). Tachie et al. (2006) investigated turbulent flow over transverse square ribs in a converging open channel. The profiles of mean velocity and turbulent quantities were obtained to document the characteristics of turbulent flow over transverse ribs in a converging open channel. The local flow structure in a rectangular duct may be dominated by transverse flow, i.e. secondary flow (Launder and Ying, 1972; Gessner, 1973; Gessner and Emery, 1981). Little is known about the structure of internal turbulent flows, even in straight ducts (Panidis and Papailiou, 2000; Su and Friedrich, 1994). Even less is known about the process by which non-spherical particles become wedged in constrictions as they flow horizontally. One type of constriction, the nozzle, has been investigated in previous studies (Islam et al., 2002; Tachie et al., 2006; Deo et al., 2007a,b). Nozzle design (e.g. diameter or aspect ratio), particle properties (e.g. size), and fluid properties and velocity are critical for smooth nozzle two-phase flow.

This paper examines the flow of groups of non-spherical particles of well-defined shape through constrictions of known shape. The intention is to provide better understanding of the principal factors which govern blockage when multiple solid particles encounter flow constrictions. Possible modes of blockage are identified in Table 1, together with a "Blockage Index" to characterize the frequency and seriousness of blockages or partial blockages.

2. Experimental set-up and methodology

A Particulate Flow Loop was designed and fabricated to investigate the fundamentals of the movement of clusters of particles of different well-characterized shapes through narrow gaps or constrictions as they are conveyed by water.

The test section is a rectangular duct, 25.4 mm wide × 66 mm high, as indicated in Fig. 1, with interchangeable narrow gaps of different shapes (ramp, circular, and rectangular). Upstream of the test section, there is a rectangular duct of the same cross-sectional dimensions and length 5.18 m. The Reynolds number based on the mean velocity of the conveying water and hydraulic diameter (D_h = 0.0367 m) of the rectangular duct ranged from ~730 to

* Corresponding author. Tel.: +1 604 827 3232; fax: +1 604 822 6003.
E-mail address: jianjuntai@gmail.com (J. Dai).

0301-9322/$ - see front matter © 2009 Elsevier Ltd. All rights reserved.
doi:10.1016/j.ijmultiphaseflow.2009.08.001

Table 1
Characterization of blockage index for swarms of particles in Particulate Flow Loop.

Blockage extent	Particulate Flow Loop	Blockage index
1	Stable blockage forms	1
2	Unstable blockage, which breaks up on its own within 5 s, without operator intervention	0.5
3	No blockage	0

44,000. The corresponding mean velocity of the water was 0.02–1.2 m/s. From previous work, the maximum development length for laminar flow in a rectangular duct is $L_e/(D_H\mathrm{Re}) = 0.09$ (Goldstein and Kreid, 1967), whereas the development length is 140 times the hydraulic diameter for turbulent duct flow (Klein, 1981). Hence fully developed flow was achieved for turbulent flow ($Re > 6000$ for rectangular ducts of aspect ratio 3:1) (Eckert and Irvine, 1957; Hartnett et al., 1962) in the rectangular duct in the present study. When $Re < 2000$, fully developed laminar flow could be achieved. For $2000 < Re < 6000$, the flow was unable to reach the fully developed state.

A screen with 0.71 mm openings was installed downstream of the test section to prevent particles from entering the pump (Model: LEESON 62RS1C-3.5, head: 15.2 m, capacity: 0.001 m^3/s). To ensure higher water flow rates and pressure, pressurized water (<572 k Pa_g, <0.005 m^3/s) was introduced into the flow loop as shown in Fig. 2. The rectangular duct was horizontal (confirmed with a level) with its centreline 39 mm above the laboratory floor. A plastic tank of capacity 300 l containing a baffle to separate the return flow region from the outlet, was installed 2.64 m above the ground. Three vent holes on the upper surface of the duct (50, 350 and 1380 mm upstream of the test section) were connected to plastic tubes to disengage air bubbles, ensuring that only water and particles (two phases) passed through the constriction.

Rubber and plastic particles (dimensions: 2–50 mm, density: 860–2100 kg/m^3) of different shapes (spheres, cylinders, disks and cuboids) were employed in the experiments, with water as the conveying fluid. Water absorption by all particles was very low (typically <1 wt% over 24 h for PTFE, and <0.03 wt% in 24 h for polyethylene particles). Therefore, changes of physical properties (e.g. density) during flow were neglected. Photos of the various particles are provided in Fig. 3. Physical properties appear in Table 2. Shore A durometer measurements (see Table 2) indicate that the rubber particles with durometer 40–70 in the present study had significant compressibility. These particles could experience elastic deformation. The particle density was obtained by putting a known mass of particles into a graduated cylinder with water (for particles with densities greater than that of water) or ethanol (for particles with densities between those of water and ethanol). By equalizing the volume before and after adding the particles to the graduated cylinder and measuring the corresponding mass, the particle volume and density were obtained.

When valves 1, 2, 3, 4 and 6 in Fig. 2 were closed and valve 5 was opened, a number of particles (typically 200) entered through the union into the section (diameter: 51 mm) above valve 3. When the union was closed tightly and valve 3 was opened, the particles descended into the flow loop. Valves 3 and 5 were then closed and valve 4 opened. Alternatively valves 1, 3 and 4 were opened and valves 2, 5 and 6 closed. The pressurized water from valves 1 and 3 carried particles into the loop. Valve 1 or 3 was shut off

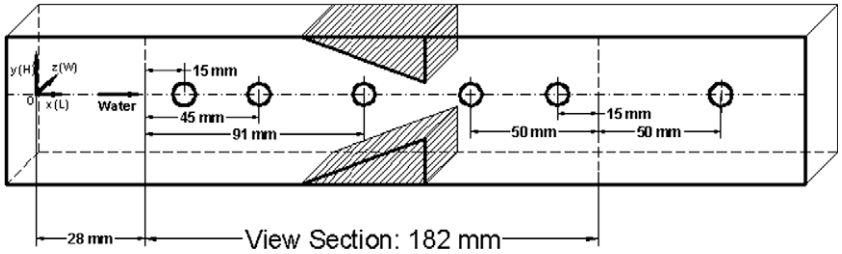

Fig. 1. Schematic of view section with ramp constriction.

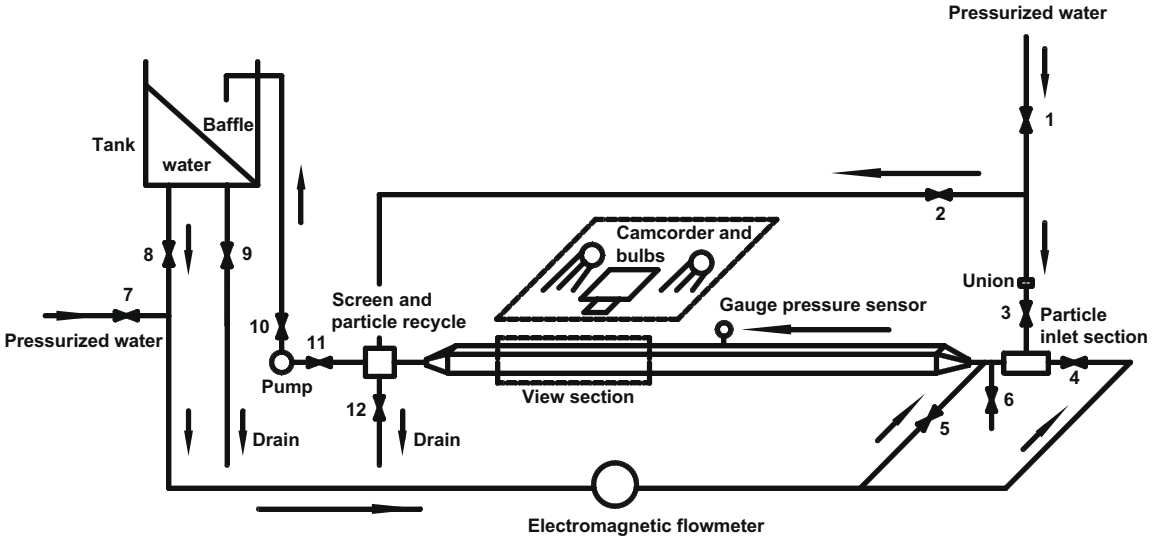

Fig. 2. Schematic of Particulate Flow Loop.

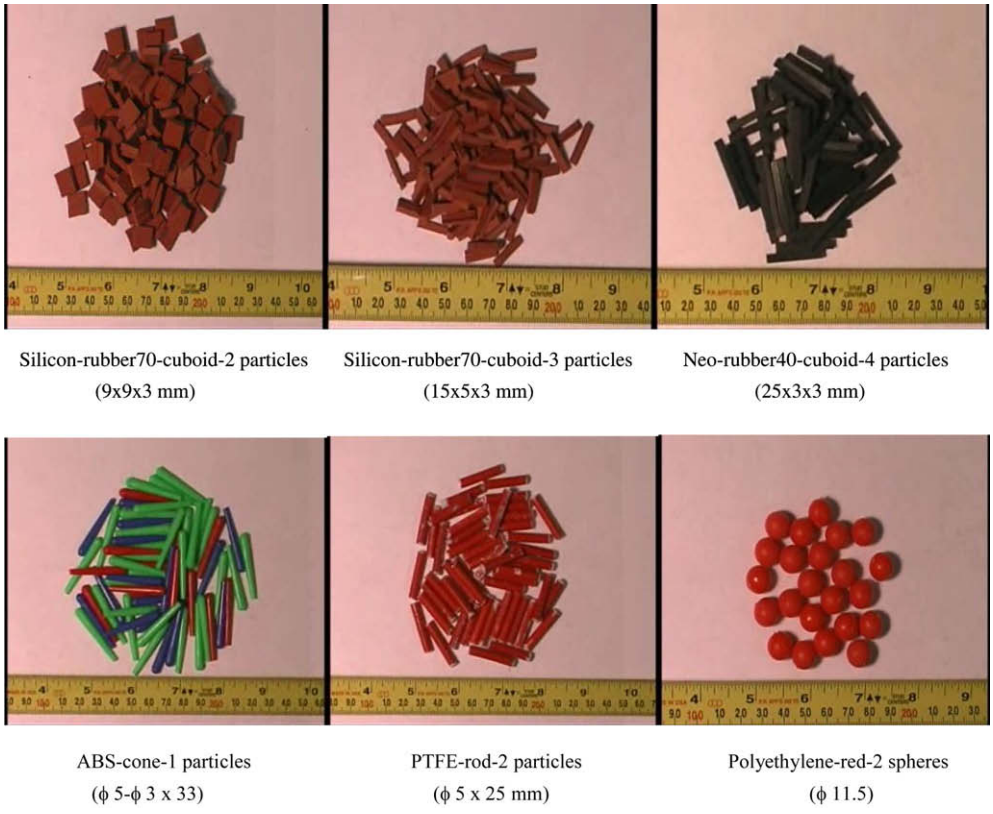

Fig. 3. Photos of main particles used in the present study.

Table 2
Particles tested in Particulate Flow Loop.

Particle type	ρ_p (kg/m^3)	Shape	Dimensions (mm)	Dv[a] (mm)	Ds[b] (mm)	Sphericity	Aspect ratio[c]	Durometer[d] (shore A)
Neo-rubber60-cuboid-0[e]	1445	Cuboid	5 (L) × 5(W) × 3 (H)	5.23	2.96	0.78	1.7	60
Neo-rubber60-cuboid-1	1445	Cuboid	7 (L) × 7(W) × 3 (H)	6.55	3.81	0.74	2.3	60
Neo-rubber60-cuboid-2	1445	Cuboid	9 (L) × 9(W) × 3 (H)	7.74	4.64	0.7	3	60
Neo-rubber60-cuboid-3	1445	Cuboid	15 (L) × 5(W) × 3 (H)	7.55	4.64	0.66	5	60
Neo-rubber60-cuboid-4	1445	Cuboid	25 (L) × 3(W) × 3 (H)	7.55	5.03	0.56	8.3	60
Neo-rubber40-cuboid-1	1080	Cuboid	5 (L) × 5(W) × 3 (H)	5.23	2.96	0.78	1.7	40
Neo-rubber40-cuboid-2	1080	Cuboid	9 (L) × 9(W) × 3 (H)	7.74	4.64	0.7	3	40
Neo-rubber40-cuboid-3	1080	Cuboid	15 (L) × 5(W) × 3 (H)	7.55	4.64	0.66	5	40
Neo-rubber40-cuboid-4	1080	Cuboid	25 (L) × 3(W) × 3 (H)	7.55	5.03	0.56	8.3	40
Nitril-rubber60-cuboid-1	1517	Cuboid	5 (L) × 5(W) × 3 (H)	5.23	2.96	0.78	1.7	60
Nitril-rubber60-cuboid-2	1517	Cuboid	7 (L) × 7(W) × 3 (H)	6.55	3.81	0.74	2.3	60
Nitril-rubber60-cuboid-3	1517	Cuboid	9 (L) × 9(W) × 3 (H)	7.74	4.64	0.7	3	60
Nitril-rubber60-cuboid-4	1517	Cuboid	25 (L) × 3(w) × 3 (H)	7.55	5.03	0.56	8.3	60
Silicon-rubber70-cuboid-0	1610	Cuboid	5 (L) × 5(w) × 3 (h)	5.23	2.96	0.78	1.7	70
Silicon-rubber70-cuboid-1	1610	Cuboid	7 (L) × 7(w) × 3 (h)	6.55	3.81	0.74	2.3	70
Silicon-rubber70-cuboid-2	1610	Cuboid	9 (L) × 9(W) × 3 (H)	7.74	4.64	0.7	3	70
Silicon-rubber70-cuboid-3	1610	Cuboid	15 (L) × 5(W) × 3 (H)	7.55	4.64	0.66	5	70
Silicon-rubber70-cuboid-4	1610	Cuboid	25 (L) × (W) × 3 (H)	7.55	5.03	0.56	8.3	70
ABS-Cone-1	1020	Cone	ϕ5–ϕ3 × 33	9.3	5.9	0.62	8.3	100
PTFE-Rod-1	2040	Cylinder	ϕ5 × 10	7.2	3.7	0.83	2	100
PTFE-Rod-2	2040	Cylinder	ϕ5 × 25	9.8	5.7	0.7	5	100
Polyethylene-red-1	1019	Sphere	ϕ11.5	11.5	11.5	1.0	1	100
Polyethylene-red-2	926	Sphere	ϕ11.5	11.5	11.5	1.0	1	100
Polyethylene-yellow-1	866	Sphere	ϕ6.4	6.4	6.4	1.0	1	100

[a] Diameter of sphere of equivalent volume.
[b] Diameter of sphere of equivalent surface area.
[c] Ratio of maximum to minimum dimension.
[d] Shore hardness is the preferred method for characterizing the hardness of rubbers/elastomers and is also commonly used for 'softer' plastics. The shore A hardness is the relative hardness of elastic materials such as rubber or soft plastics. It is determined by a Shore A durometer. If the indenter completely penetrates the sample, a reading of 0 is obtained, whereas if no penetration occurs, the reading is 100. The reading is dimensionless. High values correspond to high hardness. The hardness of relatively hard plastic particles in the present study was approximately 100.
[e] Neo denotes neoprene rubber.

within 3 s to avoid disturbing the flow in the duct. Most particles in the present study had densities greater than water. Hence, once valve 3 in Fig. 2 was opened, most particles fell immediately into the loop by gravity. However, 5–15% of the particles of irregular shape commonly deposited along the duct, from the particle inlet section to the constriction, due to corners and irregular particle shapes. Therefore, slightly more particles were put into the particle inlet section than desired to ensure that the desired number of particles passed through the constriction. Particles were re-used after being recovered from the screen. Swarms of particles were investigated to elucidate the influence of particle interactions with each other and with the gaps.

Five differential pressure transmitters (Endress + Hauser, Deltabar S PMD 230, −0.25–0.25 mH_2O) measured the pressure variation along the test section. An electromagnetic flowmeter (Endress + Hauser, promag 33) measured the mean velocity of the water. The flow visualization system included a digital video camcorder (Canon xL1), as well as a mirror and three 100 W lamps. The camcorder was connected to the serial port of a computer (Pentium III, 601 MHz, 128 MB of RAM). Data including the time from each frame were stored on the hard disk. During visualization, the laboratory lights were turned off to darken the surroundings. Three light bulbs were adjusted to a suitable brightness to give clear pictures on the viewfinder. A shutter speed of 1/1000 s was employed. The camcorder not only captured images of particle blockage, but also recorded particle trajectories. It captured simultaneous images from the front and top surfaces of the test section, aided by a mirror fixed at 45° to the horizontal to provide the top view. The video camcorder, electromagnetic flowmeter and all pressure sensors were connected to the data acquisition system.

Particle velocities were determined by timing the passage of particles between grid lines inscribed on the test section. The refractive index, n, (relative to air at 20 °C and 101.3 kPa for a wavelength of 589.3 nm) of Plexiglas is 1.491, while that of water is 1.332. Since the camcorder was directly in front of, and at some distance from, the area of interest, light refraction between the water and Plexiglas was neglected. The flow data were stored on videotape for later analysis. With image analysis software (Ulead, Pinnacle Systems DV300-Adobe Premiere LE 4.2, Adobe Photoshop 6.0 and Matlab 6.1), the data were digitized for processing. Image analysis involved:

(1) Grabbing a frame from the videotape and digitizing;
(2) inimization of background noise;
(3) sharpening of images;
(4) correcting the dimensions with the aid of the grid lines on the test section, to identify the relationship between image pixel dimensions and actual dimensions;
(5) establishing the threshold (starting point) of particle motion;
(6) identifying the edge of the particles in the images and finding the x, y and z coordinates of the particle centroid;
(7) computing the particle position and velocity at each time step (1/30 s); the number density and volume fraction of particles in each zone could also be calculated.

The particle number density is the number of particles per unit volume of the test section 0.28 (L) × 0.0254 (W) × 0.066 (H) m just upstream of the constriction, whereas the volume fraction of particles is the total particle volume divided by the volume of the same test section (length is 119 mm upstream of constriction, see Fig. 1). From image analysis, the number of particles entering and leaving the test section in each frame can be counted, so that the number of particles in the test section can be calculated. The volume of particles in the test section can be obtained from the number of particles because the volume of every particle is known. The volume of particle clusters in the test section was also based on particle number analysis.

The shapes of the ramp, circular and rectangular test sections are shown in Table 3. The surfaces of all blocks, including ramp, rectangular and circular blocks, were smooth (roughness < 0.05 mm).

3. Experimental results and discussion

All experiments were performed at least 20 times for the same particles and the same experimental conditions. Blockage indices are arithmetic average values based on the simple blockage propensity scoring scheme decided in Table 1. The local particle number density and volume fraction are important factors affecting blockage in the constriction. They were not identical in each test, even when the same particles and experimental conditions were employed. However, the differences were small for the same experimental procedures (e.g. particle injection method) with the same particles and same experimental conditions. Particle number densities in the approaching swarms of particles were in the range 8000 to $4 \times 105/m^3$, whereas particle volume fractions ranged from 0.001 to 0.1.

3.1. Effect of aspect ratio on blockage for cuboidal particles

In these tests, 200-particle groups of silicon-rubber70-cuboid-2, silicon-rubber70-cuboid-3, silicon-rubber70-cuboid-4, Neo-rubber40-cuboid-4 and Neo-rubber60-cuboid-4 were released on each occasion. The duct Reynolds number was Re = 29,700, with the water mean velocity being 0.8 m/s and rectangular constriction-1 (25.4 (W) × 12.5 (H) × 40 (L) mm). All of these particles were cuboids, with similar volume-equivalent diameters (7.74 mm for 9 × 9 × 3 mm, and 7.55 mm for the 15 × 5 × 3 and 25 × 3 × 3 mm particles). Note that the maximum dimensions of the latter two types of particles exceeded the minimum gap dimension (12.5 mm).

It was found that cuboidal silicon-rubber particles of large aspect ratio (e.g. 8.3 for 25 × 3 × 3 mm silicon-rubber70-cuboid-4 particles) were not easily transported by water. Some of these particles always deposited in the duct or blocked the gap instead of passing through the constriction. They were also more likely to block the constriction than particles of smaller aspect ratio (e.g. the 15 × 5 × 3 mm silicon-rubber70-cuboid-3 particles). On the other hand, particles of smaller aspect ratios (e.g. 9 × 9 × 3 mm silicon-rubber70-cuboid-2 particles) were generally more difficult to transport than those of larger aspect ratio (e.g. 15 × 5 × 3 mm silicon-rubber70-cuboid-3 particles) as shown in Figs. 4 and 5. It seems that there is an optimum aspect ratio for particles of the same or similar equivalent volume diameters to reduce the blockage propensity. 7 × 7 × 3 mm silicon-rubber particles of 70 durometer did not block this rectangular constriction, although a small number of these particles deposited immediately upstream of the constriction. Irregular shape particles readily deposited along the duct, and low water mean velocities (e.g. <0.6 m/s) were unable to transport these particles. Hence higher water mean velocities were employed (>0.8 m/s) to avoid deposition. Even so, a small number of particles deposited along the duct, especially in front of the constrictions. Upstream deposition is not considered to constitute blockage. Fig. 6 shows the effects of particle size and shape on blockage, demonstrating that larger particles of more irregular shapes (larger aspect ratios and smaller sphericity) were generally more likely to lodge in a given constriction.

3.2. Effect of particle density and stiffness on blockage

Neo-rubber60-cuboid-4 and Nitril-rubber60-cuboid-4 have slightly different particle densities, as shown in Table 2. This did

Table 3
Configurations of tested constrictions.

Constriction no.	Block dimensions[a]	Minimum gap dimensions[b]	Constriction shape
Ramp constriction –1 (gap between two wedges)	Length: 61 mm Maximum height: 26.8 mm Width: 25.4 mm Angle: 23.9°	Height: 12.5 mm Width: 25.4 mm	
Ramp constriction –2 (gap between two wedges)	Length: 71 mm Maximum height: 23.6 mm Width: 25.4 mm Angle: 18.4°	Height: 18.8 mm Width: 25.4 mm	
Ramp constriction –3 (gap between two wedges)	Length: 61 mm Maximum height: 20.3 mm Width: 25.4 mm Angle: 18.4°	Height: 25.4 mm Width: 25.4 mm	
Ramp constriction –4 (three-dimensional wedge gap)	Length: 61 mm; Maximum height: 23.6 mm Width: 25.4 mm Angle: 18.4°	Height: 12.5 mm Width: 12.5 mm	
Circular constriction –1 (gap between two half-cylinders)	Diameter: 26.8 mm Width: 25.4 mm	Maximum height: 12.5 mm Width: 25.4 mm	
Circular constriction –2 (gap between two half-cylinders)	Diameter: 20.3 mm Width: 25.4 mm	Maximum height:25.4 mm Width: 25.4 mm	
Rectangular constriction –1 (gap between two rectangular blocks)	Length: 40 mm Height: 26.8 mm Width: 25.4 mm	Height: 12.5 mm Width: 25.4 mm	
Rectangular constriction –2 (gap between two rectangular blocks)	Length: 40 mm Height: 20.3 mm Width: 25.4 mm	Height: 25.4 mm Width: 25.4 mm	
Rectangular constriction –3 (gap between two rectangular blocks)	Length: 20 mm Height: 26.8 mm Width: 25.4 mm	Height: 12.5 mm Width: 25.4 mm	

[a,b]Length is the dimension in the streamwise direction; height is the dimension in the vertical direction (at right angles to the flow direction); width is the dimension in the spanwise direction.

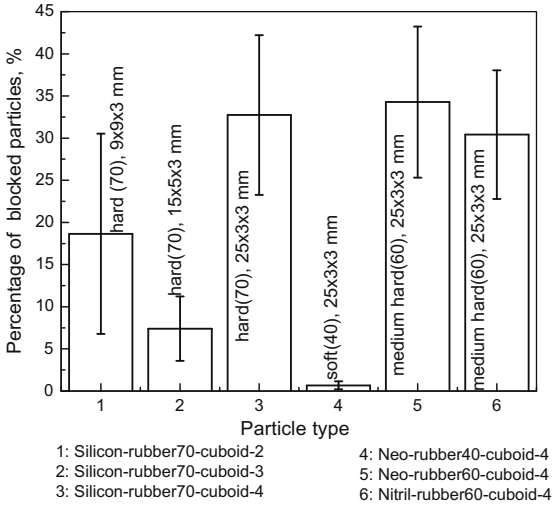

Fig. 4. Percentage of blocked particles of hardness 40, 60, 70. 200 particles released at a time, $Re = 29{,}700$, rectangular constriction-1. Bars show 95% confidence intervals.

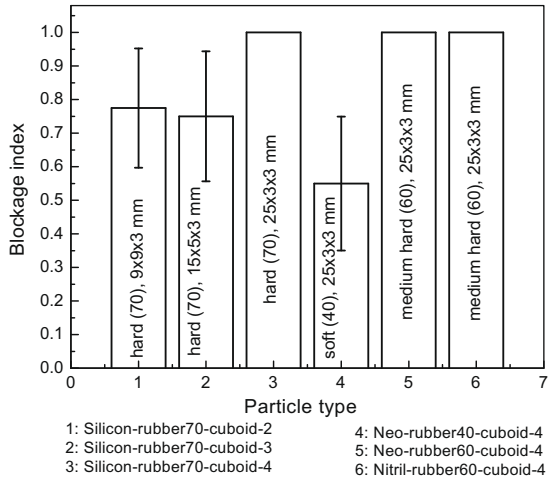

Fig. 5. Blockage index comparison for particles of hardness 40, 60 and 70. 200 particles released at a time, $Re = 29{,}700$, rectangular constriction-1. Bars show 95% confidence intervals.

not appear to cause an appreciable difference in blockage index or in deposition upstream of the constriction as shown in Figs. 4 and 5. Denser particles are expected to deposit more easily than light ones for the same geometry, dimensions, and experimental conditions. Particles less dense than water (polyethylene-red-2 and polyethylene-yellow-1 particles) were transported readily, with no deposition along the duct. However, they were more likely to be trapped in the corners upstream and downstream of the constriction. Greater flexibility of the lower-density particles made it easier for them to adjust their orientations, velocities and positions, thereby reducing the probability of blockage.

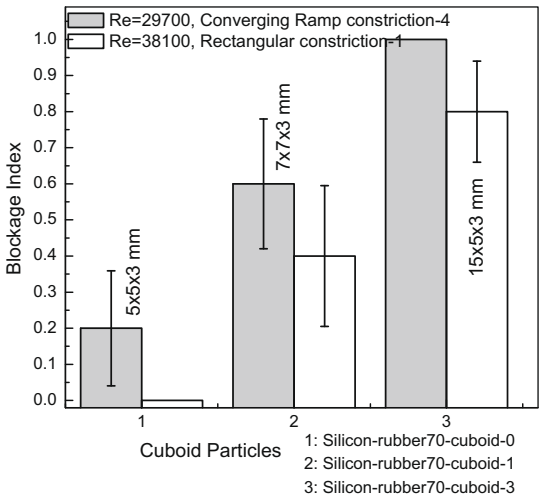

Fig. 6. Effect of particle size and shape on blockage. Injected particles each time = 400, 200, 200 for silicon-rubber70-cuboid-0, 1, 3. Bars show 95% confidence intervals. At <0.13 level, the differences of the population means differ significantly from the test difference, two samples *t*-test.

Neoprene rubber with 40 durometer was easily transported through the gap due to its low particle density. Stable blockages were less likely for soft rubber particles due to their lower bending/flexural strength, larger compressibility, and larger flexibility than for relatively hard particles, as shown in Figs. 4 and 5 (Dai, 2007). Particle number density and solid volume fraction of the particles in these tests are shown in Table 4.

3.3. Effect of constriction type and dimensions on blockage

To investigate the influence of constriction type, clusters of 160 conical ABS-cone-1 particles and of 220 silicon-rubber-cuboid-0 particles were released with $Re = 38{,}100$ ($U_m = 1.05$ m/s) to reach ramp constriction-4 (12.5 (W) × 12.5 (H) mm) and rectangular constriction-1 (25.4 (W) × 12.5 (H) mm).

The smaller converging constriction showed a greater tendency to block than the larger rectangular constriction, as shown in Fig. 7. For ramp-constriction-4, the smaller dimension in the spanwise direction than for rectangular constriction-1 led to more particle collisions with each other and with the gap, enhancing the probability of blockage.

Ramp constriction-1 and rectangular constriction-1 had the same minimum gap dimensions, i.e. 25.4 (W) × 12.5 (H) mm. 200 Neo-rubber60-cuboid-4 particles of dimensions 25 × 3 × 3 mm were released into the water flow at $Re = 29{,}700$ ($U_m = 0.8$ m/s). The maximum particle dimension (25 mm) exceeded the minimum dimension of the gap (12.5 mm). Due to the abrupt change of the dimension of rectangular constriction-1, water and particles also abruptly changed their velocities and directions of motion, promoting particle collisions with the wall and with each other, thereby increasing the likelihood of blockage. As shown in Fig. 8, the smooth convergence of ramp-constriction-1 reduced the probability of particle collisions and provided more space for particles to disentangle before reaching the minimum cross-section of the gap.

3.4. Effect of Reynolds number on blockage

The effect of water velocity and Reynolds number over limited ranges can be seen by comparing results for conical ABS-01 and cuboidal silicon-rubber70-cuboid-3 particles with the rectangular (abrupt) and ramp constrictions. Fig. 9 indicates that larger Reynolds numbers generally led to more blockage. This appears to be because higher fluid velocities tended to cause more particles to pass through the constriction simultaneously, increasing the frequency of particle collisions with each other and with the gap, in turn increasing the probability of jamming and blockage.

3.5. Effect of ratio of maximum particle dimension-to-minimum-gap-dimension

Tests were carried out for silicon-rubber70-cuboid-0, -1 and -3 particles, with release each time of 400, 200 and 200 particles, respectively. With rectangular constriction-1 (25.4 (W) × 12.5 (H) × 40 (L) mm) and ramp constriction-4 (12.5 (W) × 12.5 (H) mm), Fig. 10 shows that larger ratios of maximum particle dimension to minimum constriction dimension reduced the ability of particles to pass through the constriction, especially for ramp constriction-4, which did not provide as much space as rectangular contriction-1 in the spanwise direction. As expected, larger particles were more likely to block.

3.6. Effect of particle compressibility and flexibility

To investigate the influence of particle compressibility and flexibility, groups of 160 conical ABS-cone-1 and cuboidal silicon-

Table 4
Particle number density and solid volume fraction of particles.[a]

	PND (1/mm^3) and SVF[b]	Lower limit	Upper limit	Mean	Passing time[c] (s)
Silicon-rubber70-cuboid-1 (7 × 7 × 3 mm)	PND (mm^{-3})	1.28E−05	2.56E−04	1.34E−04	5–9
	SVF (–)	1.88E−03	3.76E−02	1.97E−02	5–9
Silicon-rubber70-cuboid-2 (9 × 9 × 3 mm)	PND (mm^{-3})	1.28E−05	2.56E−04	1.34E−04	7–11
	SVF (–)	3.11E−03	6.21E−02	3.26E−02	7–11
Silicon-rubber70-cuboid-3 (15 × 5 × 3 mm)	PND (mm^{-3})	1.28E−05	2.56E−04	1.34E−04	6–10
	SVF (–)	2.88E−03	5.75E−02	3.02E−02	6–10
Silicon-rubber70-cuboid-4 (25 × 3 × 3 mm)	PND (mm−3)	8.52E−06	1.28E−04	6.83E−05	8–16
	SVF (–)	1.92E−03	2.88E−02	1.44E+02	8–16
Neo-rubber40-cuboid-4 (25 × 3 × 3 mm)	PND (mm^{-3})	8.52E−06	1.07E−04	5.78E−05	5–7
	SVF (–)	1.92E−3	2.4E−02	1.30E−02	5–7
Neo-rubber60-cuboid-4 (25 × 3 × 3 mm)	PND (mm^{-3})	8.52E−06	1.28E−04	6.83E−05	6–10
	SVF (–)	1.92E−3	2.88E−02	1.54E−02	6–10
Nitril-rubber60-cuboid-4 (25 × 3 × 3 mm)	PND (mm^{-3})	8.52E−06	1.28E−04	6.83E−05	6–10
	SVF (–)	1.92E−3	2.88E−02	1.54E-02	6-10

[a] Number of particles released for each trial = 200, $Re = 29{,}700$.
[b] PND denotes particle number density (mm-3); SVF denotes solid volume fraction.
[c] Time for all particles to pass through the viewing section (shown in Fig. 1).

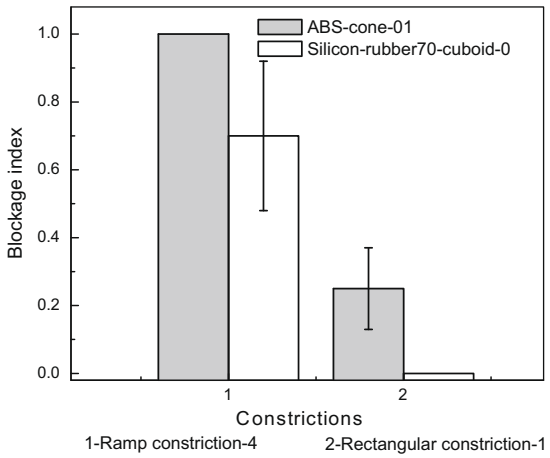

Fig. 7. Effects of constriction type and dimensions on blockage for Re = 38,100 for 160 and 220 injected particles for ABS and silicon particles, respectively. Bars show 95% confidence intervals. At the 0.001 level, the differences of the population means differ significantly from the test difference, two samples t-test.

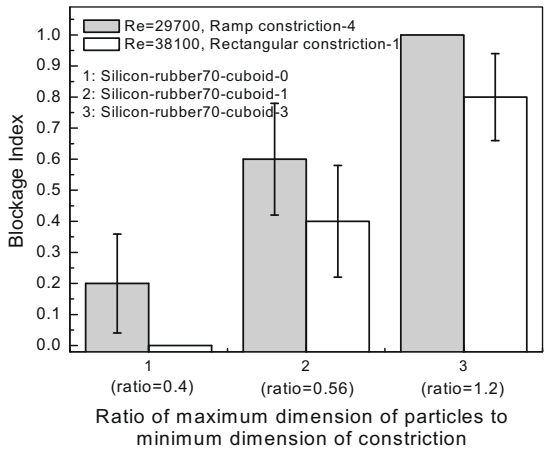

Fig. 10. Effect of ratio of maximum particle dimension to minimum constriction dimension on blockage for cuboidal rubber particles of different sizes. 400, 200, 200 particles released each time for silicon-rubber70-cuboid-0, 1, 3, respectively. Bars show 95% confidence intervals. At <0.09 level, the differences of the population means differ significantly, two samples t-test.

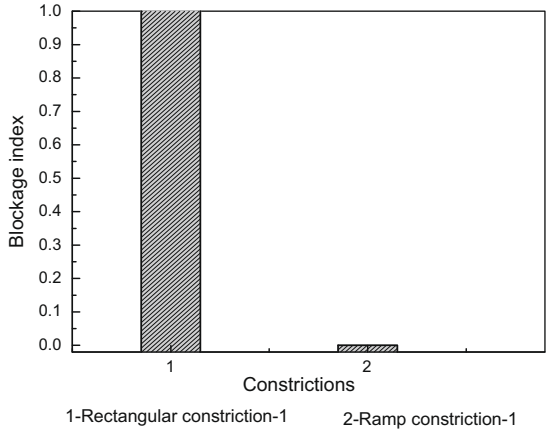

Fig. 8. Effect of constriction type and dimension on blockage for Re = 29,700. 200 Neo-rubber60- cuboid-4 particles injected each time.

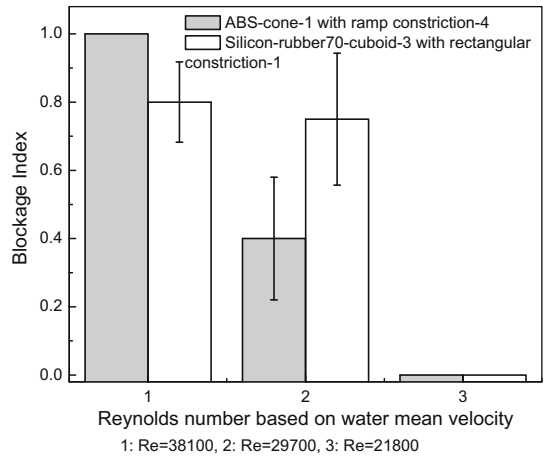

Fig. 9. Effect of Reynolds number on blockage for release of 160 and 200 particles. ABS and silicon-rubber, respectively. Bars show 95% confidence intervals. At the 0.05 level, the differences of the population means differ significantly from the test difference, two samples t-test.

rubber70-cuboid-3 particles were released to reach ramp constriction-4 (12.5 (W) × 12.5 (H) mm with Re = 29,700 (U_m = 0.8 m/s). As mentioned above, when these particles contacted each other and the gap, they tended to jam together due to compressibility, increasing the probability of blockage. Neoprene rubber particles with Shore A hardness 40 were more easily transported along the duct due to their low density, and blockages were more easily dislodged due to their pliability, flexibility (discussed below), and compressibility relative to the harder particles, as shown in Figs. 4 and 5. Particles with low bending/flexural strength and low density passed through constrictions more easily, and when they did block, the jam was more likely to break up. Compressible particles with relatively higher bending strengths and greater densities (e.g. silicon-rubber particles with 70 hardness) caused more stable blockages. Incompressible particles of relatively low density (e.g. ABS-cone-1) were more likely to pass through constrictions over the Re range (26,000 < Re < 38,000). Increased Re and intensive particle collisions increased the probability of blockage.

The ability of particles to pass through a constriction is also a function of the particle flexibility, F, defined as

$$F = \frac{1}{S} = \frac{1}{EI} \tag{1}$$

where S is the fibre stiffness in bending, E the elastic modulus, and I the area moment of inertia of the particle (Kumar, 1990).

Compressibility is inversely proportional to elastic modulus (i.e. E). Hence large compressibility leads to large flexibility for equal area moments of inertia. The larger the flexibility, the easier it is for particles to pass through constrictions. Soft rubber (e.g. 40 hardness) has a small E relative to hard rubber. For cuboid particles, the mass moment of inertia (I_h) and area moment of inertia (I_w) are respectively

$$I_h = \frac{1}{12} m(w^2 + l^2), \quad I_w = \frac{wl^3}{12} \tag{2}$$

where m is the particle mass, and h, w, and l are the height, width and length of the cuboidal particle. I_h is the mass moment of inertia about the axis in the h direction which passes through the particle centroid. Large mass and particle dimensions lead to large mass moments of inertia. The object is assumed to have uniform density. The larger the area moment of inertia, the less the particle bends.

From the particle flexibility point of view,

(1) For the same rubber, smaller particles lead to smaller area moments of inertia and greater flexibility, as indicated in Figs. 4 and 5.
(2) For the same particle dimensions, softer particles and smaller E provide greater flexibility, causing the behaviour indicated in Figs. 4 and 5.
(3) For particles of different materials, flexibility is a trade-off between area moment of inertia, elastic modulus and other particle properties (see below), as indicated in Fig. 11. ABS-cone-1 and silicon-rubber70-cuboid-3 have similar dimensions and shapes, but the latter have a greater density and smaller elastic modulus. The larger density tends to increase the mass moment of inertia, whereas the smaller elastic modulus increases the flexibility. From Fig. 11, the silicon-rubber70-cuboid-3 particles demonstrated a greater likelihood of blockage than ABS-cone-1. The silicon-rubber70-cuboid-3 particles bent more easily than the ABS-cone-1 particles, so that the former were expected to pass through the constrictions more easily than the latter. However, the experimental results showed the opposite trend. Silicon-rubber70-cuboid-3 particles with significant compressibility tended to stick together after collisions with each other and/or with the wall. The resulting "agglomerates" could not be broken up as readily by hydrodynamic forces as for the soft rubber (e.g. 40 hardness) clusters, leading to enhanced blockage. Another major reason for the enhanced blockage tendency for the silicon-rubber70-cuboid-3 particles was their large particle density, which increased their mass moment of inertia, reducing flexibility. ABS-cone-1 particles could easily adjust their orientation, position and velocity, while silicon-rubber70-cuboid-3 particles were unable to adapt to fluid acceleration as easily, thereby increasing the probability of blockage. ABS-cone-1 particles were distributed across the cross-section of the duct more uniformly than the silicon-rubber70-cuboid-3 particles due to the effects of particle density as they approached the constrictions. The former underwent intense inter-particle collisions and contact with the wall, increasing the probability of stall.

3.7. Estimation of pressure drop for blockage

Table 5 shows static pressure and centerline water velocity along streamwise direction in the test section for steady state water-particle flow without blockage (see Fig. 1) (Dai, 2007). We used a by-pass to release pressure before the test section when blockage formed and didn't measure the pressure drop needed to break up the blockage in the current experiments. For the rectangular (abrupt) constrictions investigated in the present study (see Table 3), blockage only occurred at the entrance of the constriction (zone 1 in Fig. 12(a)) when particles collided with each other and with the wall, eventually leading to blockage. For the dilute water-particle flows, no blockage was observed inside the rectangular constriction (zone 2 in Fig. 12(a)). For converging ramp constrictions, the particles blocked inside the ramp, as indicated schematically in Fig. 12(b).

Table 5
Static pressure and centerline water velocity along streamwise direction (see Fig. 1).

Position of particles along X-coordinate (m)	Static pressure (Pa g)	Centerline water velocity (m/s)
0	5800	0.305
0.043	5790	0.337
0.118	5738	0.466
0.159	5585	0.723
0.194	5546	0.776
0.26	5617	0.678

From Fig. 12, imagine that a blockage can only be broken from the rectangular regions shown by dashed lines to provide a first estimate of the pressure drop through the blockage, we consider a horizontal packed assembly of uniform packing with gravity neglected in the rectangular control surfaces shown in Fig. 12. The assembly is assumed to contain enough particles for the pressure drop to be approximated by an equation (Ergun, 1952; Nemec and Levec, 2005; Keyser et al., 2006) of form:

$$\frac{\Delta P}{L_b} = A\frac{\mu_f U_0(1-\varepsilon)^2}{\phi_s^2 d_v^2 \varepsilon^3} + B\frac{\rho_f U_0^2(1-\varepsilon)}{\phi_s d_v \varepsilon^3} \tag{3}$$

For cylindrical particles, Nemec and Levec (2005) recommend

$$A = \frac{150}{\phi_s^{3/2}}, \quad B = \frac{1.75}{\phi_s^{4/3}} \tag{4}$$

Since cylindrical particles are reasonably similar in shape to cuboidal particles (maximum aspect ratio $\gg$1), Eq. (4) was employed to estimate A and B. A void fraction of 0.5 was assumed for all irregular particles. For the superficial velocities in the present study, the particle Reynolds number

$$Re_p = \frac{d_{sv} U_0 \rho_f}{\mu_f(1-\varepsilon)} = \frac{\phi_s d_v U_0 \rho_f}{\mu_f(1-\varepsilon)} \tag{5}$$

was in the range of 1900–12,960 if the particles inside the horizontal blockage bed are assumed to be stationary. When blockage occurred, the static pressure upstream of the blockage increased abruptly. This excess pressure was released either by opening by-pass valve 6 (see Fig. 2), or by collapse of the blockage bed. Fig. 13 indicates that the higher the water superficial velocity, the larger the pressure drop across a horizontal blockage bed of given length. The larger pressure drop of silicon-rubber70-cuboid-4 (right-hand column) is mainly attributed to the extreme particle shape (low sphericity). The sphericity may also affect the void fraction, more angular (i.e. lower sphericity) particles generally leading to larger voidages (Nemec and Levec, 2005), whereas a void fraction of 0.5 is assumed above. The friction between particles and wall, as well as the interlocking characteristics and bending strength of particles, determines whether or not the blockage can be broken.

From the dimensions of the constrictions most subject to blockage in Table 3, we assume W_b = 0.0254 m and H_b = 0.0125 m. In order to break the blockage,

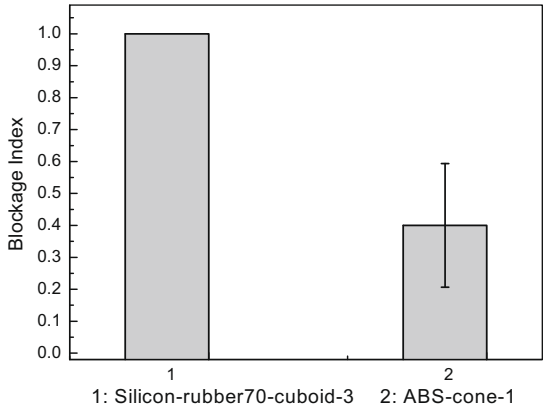

Fig. 11. Effect of compressibility of particles on blockage for warms of 160 ABS and rubber particles. Re = 29,700, ramp constriction-4. Bars show 95% confidence intervals. At the 0.001 level, the differences of the population means differ significantly, two samples t-test.

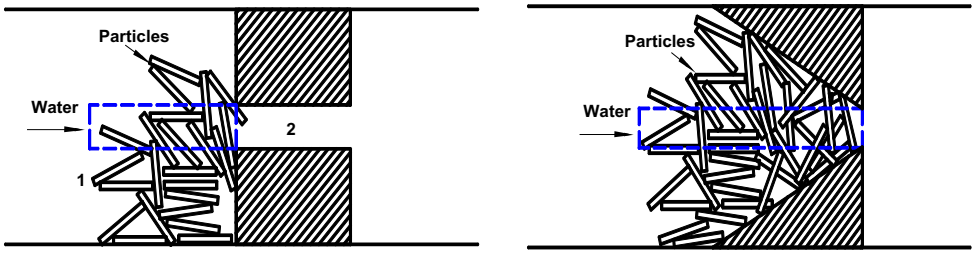

Fig. 12. Schematic of blockage in (a) rectangular (abrupt) constriction; (b) converging ramp constriction.

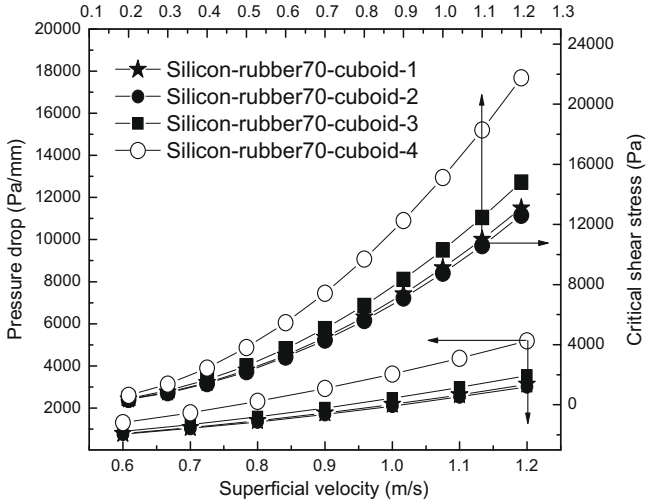

Fig. 13. Effect of superficial velocity of water on predicted pressure drop per unit length of horizontal blockage bed and critical shear stress.

$$\frac{\Delta P}{L_b} \times W_b \times H_b \geq \tau_s \times 2(W_b + H_b) \tag{6}$$

where τ_s is the average shear stress on the boundary of the blockage assembly and $\tau_s \leqslant \tau_c$, where τ_c is the critical shear stress on the boundary, calculated via.

$$\tau_c = \frac{\Delta p}{2L_b(W + H_b)} \times W_b \times H_b \tag{7}$$

Calculated shear stresses, plotted in Fig. 13, are in the range of 350–22,000 Pa, depending on the superficial water velocity, particle properties and packing characteristics of the blockage assembly. When the average shear stress at the boundary is less than the critical shear stress, the blockage tends to collapse. Note that the average shear stress may be generated either by particle–wall friction or interlocking of particles at the boundary of the horizontal blockage. As the superficial water velocity increases, the blockage assembly becomes more and more compact (i.e. void fraction decreases), increasing the shear stress required to break the blockage. Hydrodynamic forces cannot dislodge all blockages, especially when the blockage is tight. Mechanical means may then be required to force the particles through the constriction (Dai, 2007). Due to the effect of gravity, the packing of particles with $\rho_p \neq \rho_w$ tends to be non-uniform. For $\rho_p > \rho_w$, the upper part of the blockage assembly is more easily broken.

4. Conclusions

(1) Spherical particles of small size and low density were easily transported and unlikely to block constrictions, whereas irregular rubber and plastic particles of density greater than water were difficult to convey. With increasing water mean velocity, particles experienced creep, saltation and suspension.

(2) Larger particles of higher aspect ratio and density were more difficult to transport. These particles were also more likely to block the constriction at high *Re*.

(3) The maximum particle dimension does not solely determine whether or not blockage occurs when the orthogonal dimensions of the particles are such that the particles can pass through the constriction. Large particles were more likely to cause blockage. A lower particle concentration is required to block a constriction for larger than for smaller particles.

(4) Nearly neutrally buoyant conical particles (e.g. ABS-Cone-1) were more likely to block a constriction at a high water mean velocity. This appears to be mainly because of the unbalanced shape (i.e. conical), intense fluid-particle and particle–particle interactions, and a large ratio of maximum particle dimension to minimum constriction dimension.

(5) Compressible particles were more likely to block constrictions than incompressible ones, because the former tended to jam together instead of separating after colliding. However, blockage formed by soft particles tended to disengage due to their low hardness, low resistance to bending and high flexibility.

(6) Reynolds number affects particle motion and blockage tendency. For higher water mean velocities, more and more heavier non-spherical particles were transported and lifted vigorously, increasing the probability of different particles passing through the constriction simultaneously, augmenting the probability of blockage. On the other hand, as U_m increased, blockages were less likely and more readily broken, especially for small particles, because of increased drag and increased pressure gradient immediately upstream of the constriction. The probability of blockage depends on the interactions among the fluid, particles and constriction.

(7) Ramp constriction-4 with a square gap (12.5 (W) × 12.5 (H) mm) in the middle was more likely to block than a rectangular constriction-1 (25.4 (W) × 12.5 (H) mm) because the latter provides more space for particles to disperse laterally.

(8) Flow properties of the water upstream of the constriction, constriction configurations and particle properties (dimensions, shape, density, etc.) determined whether or not particles proceed directly downstream. Large particles denser than water were not readily trapped by the vortex immediately downstream of the constriction, especially at larger *Re*, because of their dimensions and inertia.

(9) Particles of larger densities and dimensions were more likely to collide with the block surface and with each other. Such collisions led to more rotation, causing abrupt changes in particle trajectories and velocities. The larger or heavier the particles, the greater the chance of them colliding with

the wall and with each other because of inertial effects. Blockage cannot occur without particle–particle and particle–wall interactions.

References

Beavers, G.S., Sparrow, E.M., Magnuson, R.A., 1970. Experiments on hydrodynamically developing flow in rectangular ducts of arbitrary aspect ratio. Int. J. Heat Mass Transfer 13, 689–702.

Dai, J., 2007. Biomass granular feeding for gasification and combustion. Ph.D. Thesis. University of British Columbia, Vancouver, Canada.

Deo, R.C., Nathan, G.J., Mi, J., 2007a. Comparison of turbulent jets issuing from rectangular nozzles with and without sidewalls. Exp. Therm. Fluid Sci. 32, 596–606.

Deo, R.C., Mi, J., Nathan, G.J., 2007b. The influence of nozzle aspect ratio on plane jets. Exp. Therm. Fluid Sci. 31, 825–838.

Eckert, E.R.G., Irvine Jr., T.F., 1957. Incompressible friction factor, transition and hydrodynamic entrance length studies of ducts with triangular and rectangular cross sections. In: Proceedings of the Fifth Midwestern Conference on Fluid Mechanics, Michigan.

Ergun, S., 1952. Fluid flow through packed columns. Chem. Engng. Prog. 48, 89–94.

Fleming, D.P., Sparrow, E.M., 1969. Flow in the hydrodynamic entrance region of ducts of arbitrary cross section. J. Heat Transfer, Trans. ASME 91, 345–354.

Gessner, F.B., 1973. The origin of secondary flow in turbulent flow along a corner. J. Fluid Mech. 58, 1–25.

Gessner, F.B., Emery, A.F., 1981. The numerical prediction of developing turbulent flow in rectangular ducts. J. Fluids Engng., Trans. ASME 103, 445–455.

Gessner, F.B., Po, J.K., 1976. A Reynolds stress model for turbulent corner flows-part II: comparisons between theory and experiment. J. Fluids Engng., Trans. ASME, 269–276.

Goldstein, R.J., Kreid, D.K., 1967. Measurement of laminar flow development in a square duct using a Laser-Doppler flowmeter. J. Appl. Mechan., 813–818.

Hartnett, J.P., Kou, J.C.Y., McComas, S.T., 1962. A comparison of predicted and measured friction factors for turbulent flow through rectangular ducts. Trans. ASME, 82–88.

Islam, M.S., Haga, K., Kaminaga, M., Hino, R., Monde, M., 2002. Experimental analysis of turbulent flow structure in a fully developed rib-roughened rectangular channel with PIV. Exp. Fluids 33, 296–306.

Keyser, M.J., Conradie, M., Coertzen, M., Van Dyk, J.C., 2006. Effect of coal particle size distribution on packed bed pressure drop and gas flow distribution. Fuel 85, 1439–1445.

Klein, A., 1981. Review: turbulent developing pipe flow. J. Fluids Engng. 103, 243–249.

Kaushal, D.R., Tomita, Y., 2003. Comparative study of pressure drop in multisized particulate slurry flow through pipe and rectangular duct. Int. J. Multiphase Flow 29, 1473–1487.

Kumar, A., 1990. Passage of fibres through screen apertures. Ph.D. Thesis. University of British Columbia, Vancouver, Canada.

Launder, B.E., Ying, W.M., 1972. Secondary flows in ducts of square cross section. J. Fluid Mech. 54, 289–295.

Melling, A., Whitelaw, J.H., 1976. Turbulent flow in a rectangular duct. J. Fluid Mech. 78, 289–315.

Nemec, D., Levec, J., 2005. Flow through packed bed reactors: 1. Single-phase flow. Chem. Eng. Sci. 60, 6947–6957.

Panidis, T., Papailiou, D.D., 2000. The structure of two-phase grid turbulence in a rectangular channel: an experimental study. Int. J. Multiphase Flow 26 (8), 1369–1400.

Sparrow, E.M., Hixon, C.W., Shavit, G., 1967. Experiments on laminar flow development in rectangular ducts. J. Basic Eng., Trans. ASME 89, 116–124.

Su, M.D., Friedrich, D., 1994. Investigation of fully developed turbulent flow in a straight duct with large eddy simulation. J. Fluids Eng., Trans. ASME 116, 677–684.

Tachie, M.F., Agelinchaab, M., Shah, M., 2006. Turbulent flow over square ribs in an open channel. In: Proceeding of the International Symposium on Turbulence, Heat and Mass Transfer. Dubrovnik, Croatia.

Wilmarth, T., Ishii, M., 1994. Two-phase flow regimes in narrow rectangular vertical and horizontal channels. Int. J. Heat Mass Transfer 37, 1749–1758.